Development of Particle Morphology in Emulsion Polymerization. 3. Cluster Nucleation and Dynamics in Polymerizing Systems

Luis J. González-Ortiz[†] and José M. Asua*

Grupo de Ingeniería Química, Departamento de Química Aplicada, Facultad de Ciencias Químicas, Universidad de País Vasco, Apdo. 1072, 20080 San Sebastián, Spain

Received January 8, 1996; Revised Manuscript Received April 2, 1996[⊗]

ABSTRACT: A mathematical model for the development of the particle morphology in emulsion polymerization has been developed. The model accounts for phase separation leading to cluster nucleation, polymerization, polymer diffusion, and cluster migration. The model has been used to simulate batch emulsion polymerizations of methyl methacrylate on a polystyrene seed for which experimentally determined particle morphologies have been reported. A good agreement between experimental results and model predictions was achieved. On the other hand, sensitivity analysis showed that the final particle morphology was not significantly affected by either the initial cluster volume or the cluster nucleation rate constant.

Introduction

The performance of composite latex particles in a given application is determined by their morphology. The morphology of the polymer particle is determined by the interplay of kinetics and thermodynamics and occurs through the following series−parallel processes:[1]

(a) The polymer chains are formed at a given position in a polymer particle.

(b) If the newly formed polymer is incompatible with the polymer already existing in the position in which it is formed, phase separation occurs. Phase separation leads to the formation of clusters.

(c) In order to minimize the Gibbs free energy, the clusters migrate toward the equilibrium morphology. During this migration, the size of the clusters may vary by (i) polymerization of the monomer inside the cluster, (ii) diffusion of polymer into or from the cluster, and (iii) coagulation with other clusters. Both the diffusion of polymer chains and the movement and coagulation of the clusters depend strongly on the viscosities of the phases.

Several mathematical models for the prediction of the particle morphology have been reported.[2−15] They consider only limiting situations in which either the polymer chains do not move from the point in which they are formed[2−8] or the polymer chains and the clusters are completely mobile and the equilibrium morphology is instantaneously reached.[9−15] However, there is experimental evidence that incompatible polymer chains do move from the point in which they are formed and that nonequilibrium morphologies are formed.[10−12,16−26]

The goal of the present series of papers is to develop a mathematical model able to predict the development of the latex particle morphology by taking into account all the relevant kinetic and thermodynamics effects. In the first paper of the series,[1] a model for cluster migration in a nonreacting system was developed. A composite particle in which clusters of polymer 1 were dispersed in a matrix of polymer 2 at a temperature above the glass transition temperature of both polymers was assumed to be the initial state. Although both van der Waals and Brownian forces act on the clusters, it has been reported that the Brownian forces are negligible as compared with the van der Waals forces,[26] and hence the actual motion of the clusters was due to the balance between the van der Waals forces and the viscous forces. In the second paper,[26] the model was extended by considering that the polymerization occurs concurrently with cluster migration. In this model, the seeded emulsion polymerization of monomer 1 on a seed of polymer 2 already containing a number of equal size tiny clusters of polymer 1 randomly distributed in each polymer particle was considered. Although the total volume of these initial clusters was negligible compared with the total amount of polymer 1 in the particle at the end of the polymerization, this was a limitation of the model because the evolution of the particle morphology was partially determined by the choice of the initial state. In addition, the monomer mass transfer rate was assumed to be high enough to maintain the monomer concentrations in the different phases at their thermodynamic equilibrium values. The effect of the monomer swelling on both interfacial tensions and viscosity was taken into account. The polymer 1 formed in the matrix was assumed to diffuse instantaneously into the clusters, its distribution between clusters being proportional to the cluster−matrix interfacial area of each cluster.

In the present work, the model is extended by considering cluster nucleation and polymer chain diffusion.

Theory

Let us consider a seeded emulsion polymerization of monomer 1 on a seed of polymer 2. As polymerization proceeds, the concentration of polymer 1 increases, and eventually phase separation occurs. The evolution of the process can be illustrated by means of the phase diagram presented in Figure 1. In the diagram, the equilibrium tie lines are roughly horizontal because the monomer swells both phases to almost the same extent. Point A represents the initial state. As monomer 1 polymerizes, the particle composition moves along the line A−B. This line will be straight if no monomer 1 enters the polymer particle after the beginning of the polymerization (i.e., batch seeded emulsion polymerization without monomer droplets in the reactor). When the system reaches point B,

* To whom correspondence should be addressed. E-mail: QPPASGOJ@SQ.EHU.ES.

[†] On leave from Universidad de Guadalajara, Guadalajara, México.

[⊗] Abstract published in *Advance ACS Abstracts,* May 15, 1996.

S0024-9297(96)00022-8 CCC: $12.00

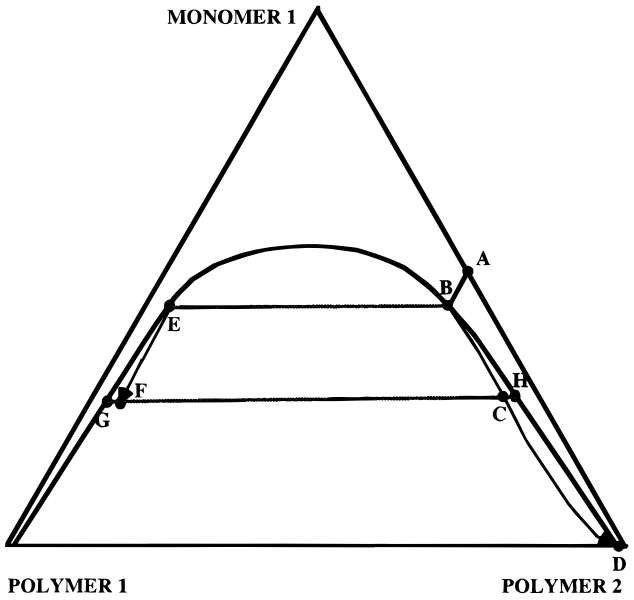

Figure 1. Phase diagram.

the polymers are no longer compatible, and phase separation occurs. However, if the kinetics of the phase separation is slower than that of the polymerization, the composition of the polymer matrix evolves along the line B−C−D, reaching the point D at the end of the polymerization. If the phase separation is quick as compared to the polymerization process, the polymer matrix moves from B to D along the equilibrium line. The composition of the first cluster formed is given by point E. Polymerization of monomer 1 in the cluster may move the composition of this cluster along the trajectory E−F, namely, off of the equilibrium line. However, the composition of the new clusters is always given by the equilibrium values. For example, point G gives the composition of the clusters formed when the composition of the polymer matrix is represented by point C. This means that, at a given moment, clusters of different compositions might be present in the polymer particle. It has to be pointed out that if a cluster formed at point E moved to point F, phase separation would occur within the cluster. However, this phenomenon was not taken into account in the model.

Cluster Nucleation. It is assumed that the rate of cluster nucleation in the polymer matrix is proportional to the excess of polymer 1 in this phase with respect to the equilibrium conditions. In particular, the flow rate of polymer 1 leaving the matrix because of cluster nucleation when the composition of the matrix is given by point C (see Figure 1) is assumed to be given by the following phenomenological relationship:

$$\frac{dV^{m}_{n_1}}{dt} = k_n(\phi_1^H - \phi_1^C) \tag{1}$$

where $dV^{m}_{n_1}dt$ is the instantaneous volumetric rate of polymer 1 leaving the polymer matrix by cluster nucleation, k_n is the rate constant of the process, and ϕ_1^C and ϕ_1^H are the volume fractions of polymer 1 at points C and H, respectively. The volumetric flow rate of polymer 2 leaving the matrix by cluster nucleation is given by

$$\frac{dV^{m}_{n_2}}{dt} = \frac{\phi_2^G}{\phi_1^G}\left\{\frac{dV^{m}_{n_1}}{dt}\right\} \tag{2}$$

where ϕ_i^G is the volume fraction of the component i under the conditions given by point G. Assuming that the initial volume of the clusters is V_C, the rate of cluster nucleation can be calculated from eq 1 as follows:

$$\frac{dN}{dt} = \frac{1}{\phi_1^G V_c}\left\{\frac{dV^{m}_{n_1}}{dt}\right\} \tag{3}$$

where N is the number of clusters. Because the number of clusters cannot be a fractional number at any time, the actual number of clusters generated was assumed to be N^*, the integer part of N:

$$N^* = \mathrm{Int}\{N\} \tag{4}$$

Since a uniform distribution of radicals was considered, the new clusters have the same probability of being located at any position in the particle. The actual position was chosen randomly using a random number generator.

Polymer Diffusion. When the system is under nonequilibrium conditions, the polymers diffuse between the matrix phase and the clusters. The rate at which polymer i diffuses into the cluster j located at point F in Figure 1 is accounted for by means of the following phenomenological equation:

$$\frac{dV^{j}_{d_i}}{dt} = \{-k^1_{di}(\phi_i^F - \phi_i^G) + k^2_{di}(\phi_i^C - \phi_i^H)\}a_j \tag{5}$$

where dV^{j}_{di}/dt is the volumetric flow rate of polymer i into the cluster j, $k^1_{d_i}$ and $k^2_{d_i}$ are the mass transfer coefficients, and a_j is the interfacial area of cluster j. The rate of diffusion of polymer i into the polymer matrix is as follows:

$$\frac{dV^{m}_{d_i}}{dt} = -\sum_{j=1}^{N^*}\frac{dV^{j}_{d_i}}{dt} \tag{6}$$

Polymerization. Polymerization occurs in both clusters and the polymer matrix. The polymer formed by polymerization in cluster j is

$$\frac{dV^{j}_{p_1}}{dt} = k_p[M_1]_j\frac{v_j}{v_P}\frac{\bar{n}}{N_A}\frac{P_M}{1000\rho_{p_1}} \tag{7}$$

$$\frac{dV^{m}_{p_1}}{dt} = k_p[M_1]_m\frac{v_m}{v_P}\frac{\bar{n}}{N_A}\frac{P_M}{1000\rho_{p_1}} \tag{8}$$

where $dV^{j}_{p_1}/dt$ and $dV^{m}_{p_1}/dt$ are respectively the volumetric generation rate of the polymer 1 in cluster j and in the polymer matrix, v_j is the volume of cluster j, v_P is the volume of monomer-swollen polymer particle, v_m is the volume of the polymer matrix, $[M_1]_j$ and $[M_1]_m$ are the concentrations of monomer 1 in the cluster j and in the polymer matrix, k_p is the propagation rate constant, $\bar{n}$ is the average number of radicals per particle, N_A is Avogadro's number, P_M is the molecular weight of monomer 1, and ρ_{p_1} is the density of polymer 1.

The concentrations of monomer 1 in the different phases were calculated by solving the equilibrium equations and the overall material balances. A detailed description of those calculations was given in the second paper of this series[26] and for the sake of brevity will not be repeated here.

Material Balances. The material balance for monomer 1 in the reactor is

$$\frac{dM_1}{dt} = k_pN_P\left\{\frac{v_m}{v_P}[M_1]_m\frac{\bar{n}}{N_A} + \sum_{j=1}^{N^*}\frac{v_j}{v_P}[M_1]_j\frac{\bar{n}}{N_A}\right\} + F_{M_1} \tag{9}$$

where M_1 is the amount of monomer 1 in the reactor, N_P is the number of polymer particles in the reactor; and F_{M_1} is the molar feed rate of monomer 1.

The balances of the polymers in the cluster j may be written as follows:

$$\frac{dV^{j}_1}{dt} = \frac{dV^{j}_{p_1}}{dt} + \frac{dV^{j}_{d_1}}{dt} \tag{10}$$

$$\frac{dV^{j}_2}{dt} = \frac{dV^{j}_{d_2}}{dt} \tag{11}$$

The initial conditions for eqs 10 and 11 are the amount of each polymer contained by the cluster when it was formed. These amounts are given by the compositions in the left-hand-side equilibrium tie line in Figure 1 and the initial volume of the cluster. Note that the balance of polymer 1 considers both diffusion and polymerization, while the balance of polymer 2 only accounts for diffusion.

The balances of the polymers in the polymer matrix may be written as follows:

$$\frac{dV_1^m}{dt} = \frac{dV_{p_1}^m}{dt} + \frac{dV_{d_1}^m}{dt} - \frac{dV_{n_1}^m}{dt} \tag{12}$$

$$\frac{dV_2^m}{dt} = \frac{dV_{d_2}^m}{dt} - \frac{dV_{n_2}^m}{dt} \tag{13}$$

The balance of polymer 1 considers polymerization, diffusion, and nucleation, while the balance of polymer 2 includes only diffusion and nucleation. Equations 10−13 assume volume additivity of the components.

Cluster Dynamics. To minimize the Gibbs free energy, the clusters migrate toward the equilibrium morphology. During the migration, the size of the clusters may increase by coagulation with other clusters (in addition to the effects of both polymerization in the clusters and polymer diffusion discussed above). A mathematical model for the motion and coagulation was presented in the first paper of this series,[1] where the details of the model can be found. However, to clarify the present paper, a summary of that mathematical model is presented here.

Although both van der Waals and Brownian forces act on the clusters, Brownian forces are negligible as compared with the van der Waals forces,[26] and hence the motion of the clusers is due to the balance between the van der Waals attraction−repulsion forces and the resistance to flow that arises from viscous drag. For small movements, the equation of motion reduces to[1]

$$\mathbf{X}_j = \mathbf{X}_{j0} + \frac{\mathbf{F}_j t}{b_j \mu} \tag{14}$$

where $\mathbf{X}_j$ is the vector giving the position of the cluster j, $\mathbf{F}_j$ is the net van der Waals force acting on the cluster j, μ is the viscosity of phase 2, t is the time, and b_j is the friction factor of the cluster j. The present paper deals with spherical and elliptical clusters (internal and superficial clusters, respectively). The friction factors for these geometries are given elsewhere.[1,26,27]

The net van der Waals force is given by

$$\mathbf{F}_j = \mathbf{F}_{j3} + \sum_{h=1,h\neq j}^{N^*} \mathbf{F}_{jh} \tag{15}$$

where N^* is the total number of clusters, and $\mathbf{F}_{jh}$ and $\mathbf{F}_{j3}$ are respectively the forces on the cluster j resulting from the interactions between the clusters j and h and between the cluster j and the aqueous phase. These forces can be obtained from the energies of interaction, E_j, using the following equation:[28]

$$\mathbf{F}_j = -\nabla E_j \tag{16}$$

The energy of interaction between two bodies depends on the shape and size of the bodies, their chemical nature, and the phase between the bodies. The shape of the cluster is the shape that minimizes the interfacial energy around the cluster. The calculation of the equilibrium morphologies, as well as the equations for the interaction energies, are given in the first paper of this series.[1] The values of the Hamaker constants required to calculate the interaction energies can be estimated from the interfacial tensions.[1] The interfacial tensions depend on the extent of the swelling. Following Chen et al.,[11] the interfacial tensions between the two polymeric phases, σ_{12}, was calculated by means of the model proposed by Broseta et al. [29]

Table 1. Recipes Used for the Simulations

	run		
	1	2	3
polymer seed (cm^3)	68.1	48.0	69.0
MMA (cm^3)	143.4	74.4	107.0
water (cm^3)	788.5	877.6	824.0
d_{seed} (m)	190×10^{-9}	725×10^{-9}	585×10^{-9}
N_P	1.9×10^{16}	2.4×10^{14}	6.6×10^{14}
T (K)	343	333	333

In addition, following Winzor and Sundberg,[13] the interfacial tensions between the polymers and the aqueous phase were calculated using the model proposed by Siow and Patterson.[30] The details of these calculations are given in the second paper of this series.[26]

Because the time scale for coagulation is generally shorter than the time scale for motion of the clusters,[1] it was assumed that the instantaneous coagulation of the clusters occurred when the surfaces of the clusters are closer than a critical arbitrary distance, d_c.

The viscosity at near-zero shear rate was estimated as follows:[31]

$$\mu = \frac{\mu_0^* \exp\left\{\frac{E_\mu}{R}\left(\frac{1}{T} - \frac{1}{T_R}\right)\right\} C^{5.4} M^{3.4}}{C_R^{\,5.4} M_R^{\,3.4}} \tag{17}$$

where μ_0^* is the viscosity at reference values of temperature, T_R, M_R is the polymer 2 molecular weight, C_R is the and concentration of polymer 2, and T, M, and C are the actual temperature, polymer 2 molecular weight, and concentration of polymer 2, respectively.

The integration was carried out using a finite difference method in which the time interval was adjusted in such way that no cluster was allowed to move more than 0.5 nm in one time interval.

Simulated Versus Experimental Particle Morphologies

Polymerization of methyl methacrylate (MMA) on a polystyrene (pSt) seed using the recipes given in Table 1 was considered. Run 1 tried to reproduce the polymerization of MMA on a polystyrene seed using Pluronic F-108 as an emulsifier as reported by Chen et al.[17] It was assumed that the whole population of particles was represented by one particle. The parameters used in the simulations are given in Table 2. $k_{d_1}^1$, $k_{d_2}^1$, $k_{d_1}^2$, and $k_{d_2}^2$ were adjustable parameters, and the rest of parameters were taken from the literature. The Hamaker constants were estimated from the interfacial tensions using the approach detailed in ref 1. It was assumed that the radicals were uniformly distributed in the polymer particles; i.e., radical concentration profiles in the polymer particles due to the anchoring of the entering radicals to the particle surface were not considered. The average number of radicals per particle, $\bar{n}$, can be calculated from the balance of radicals both in the aqueous phase and in the polymer particles, but as the parameters involved in these balances cannot currently be predicted, ab initio calculations of $\bar{n}$ are uncertain. Therefore, constant values of $\bar{n}$ were used in the simulations. These values were chosen to reach the final conversion at a time similar to that used in the experiments. Phase separation depends of the specific phase diagram of the system that in turn depends on the species involved, the molecular weight of the polymers, and the temperature. Because the molecular weights of the polymers were not reported by Chen et al.,[17] two phase diagrams were calculated. The first one used the method proposed by Hsu and Prautsnitz[32] and the following parameter values: χ_{01}

Table 2. Parameters Used in the Simulations

	run		
	1	2	3
k_n, m^3/s[a]	3×10^{-22}	2×10^{-20}	1×10^{-20}
V_C, m^3 [a]	3.6×10^{-24}	2.0×10^{-22}	1.1×10^{-22}
$k^1_{d_1}$, m/s[b]	1×10^{-9}	50×10^{-9}	4×10^{-9}
$k^1_{d_2} = k^1_{d_j}$; $k^2_{d_i} = k^1_{d_i}$[b]			
phase diagram: line a in Figure 2			

A	227[c]	M_R	2.5×10^5 g/mol[d]
B	−0.615[c]	E_μ	7000 J/mol[d]
R_g	8.77×10^{-8} m[c]	T_R	493 K[d]
μ^*_0	5×10^3 Pa s[d]	C_R	1050 kg/m^3 [d]

$$k_p = 8.7 \times 10^2 \exp\left\{\frac{-19700 \text{ J/mol K}}{RT}\right\}, \left(\frac{\text{m}^3}{\text{mol s}}\right)^e$$

$\chi_1 = 0.95$[f]
$\chi_2 = 1.0$[f]
$\sigma^*_{M3} - \sigma^*_{i3} = 2.1 \times 10^{-3}$ N/m[f]
$\sigma^*_{M3} - \sigma^*_{j3} = 2.7 \times 10^{-3}$ N/m[f]

[a] Arbitrary values, modified during the sensitivity analysis. [b] Adjustable parameters. [c] Chen et al.[11] [d] Van Krevelen.[31] [e] Walling.[34] [f] Estimated by fitting the experimental data reported Chen et al.,[11] using the model proposal by Siow and Patterson.[30]

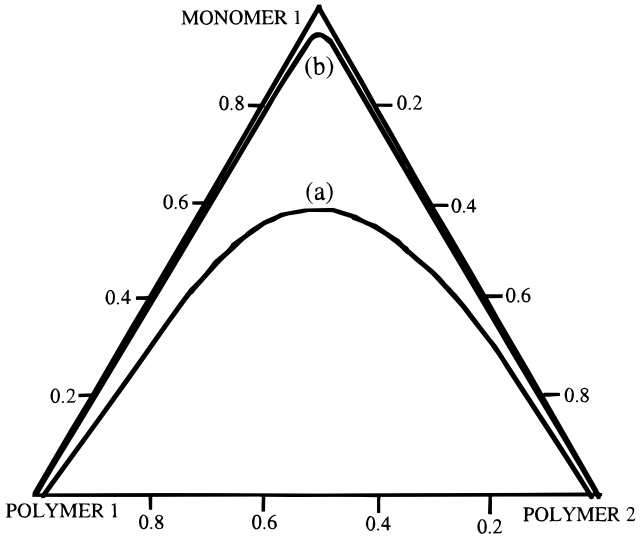

Figure 2. Phase diagram considered in the simulations. (a) $\chi_{01} = 0.40$; $\chi_{02} = 0.44$; $\chi_{12} = 0.004$; $\bar{X}_0 = 1$; $\bar{X}_1 = \bar{X}_2 = \bar{X}_n = 1000$;[32] (b) $\chi_{01} = 0.40$; $\chi_{02} = 0.40$; $\chi_{12} = 0.04$; $\bar{X}_0 = 1$; $\bar{X}_1 = \bar{X}_2 = \bar{X}_n = 1000$. [33]

$= 0.40$; $\chi_{02} = 0.44$; $\chi_{12} = 0.004$; $\bar{X}_0 = 1$; $\bar{X}_1 = \bar{X}_2 = \bar{X}_n = 1000$. The second one used the method proposed by Flory[33] and the following parameter values: $\chi_{01} = 0.40$; $\chi_{02} = 0.40$; $\chi_{12} = 0.04$; $\bar{X}_0 = 1$; $\bar{X}_1 = \bar{X}_2 = \bar{X}_n = 1000$. The first set of parameters corresponds to a system that is partially compatible and the second to an almost incompatible one. Both phase diagrams are included in Figure 2.

Figures 3−5 present the evolution of the particle morphology predicted by the model for run 1 in Table 1, together with some drawings representing the particle morphologies reported by Chen et al.[17] These authors determined the morphology of the particles by immersing the sample in liquid nitrogen and examining it by TEM. Therefore, they observed a projection of the whole particle on a plane. The simulated figures are projections of the clusters on a vertical plane that rotates 180° about the vertical axis of the polymer particles.

Figure 3 presents the evolution of the particle morphology predicted by the model for the initial stages of run 1 and an illustrative drawing of the particle

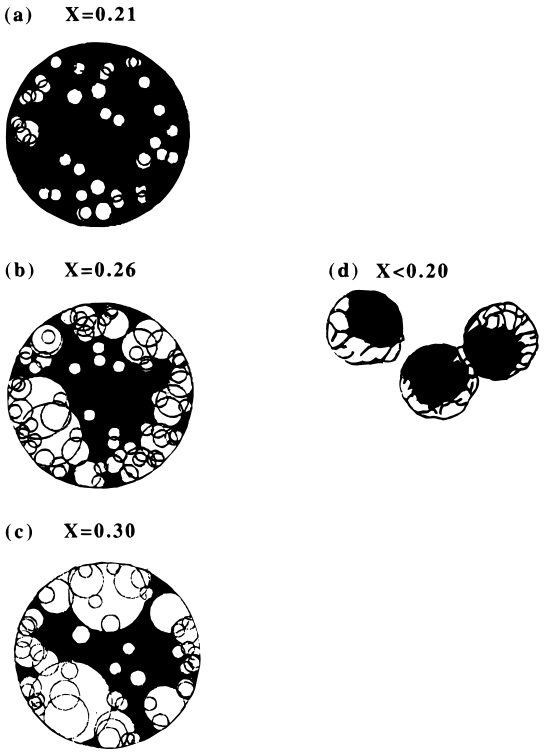

Figure 3. Comparison of the initial stages of the evolution of the particle morphology predicted by the model for run 1 in Table 1 (a−c) and the experimental morphology observed by Chen et al.[17] (d).

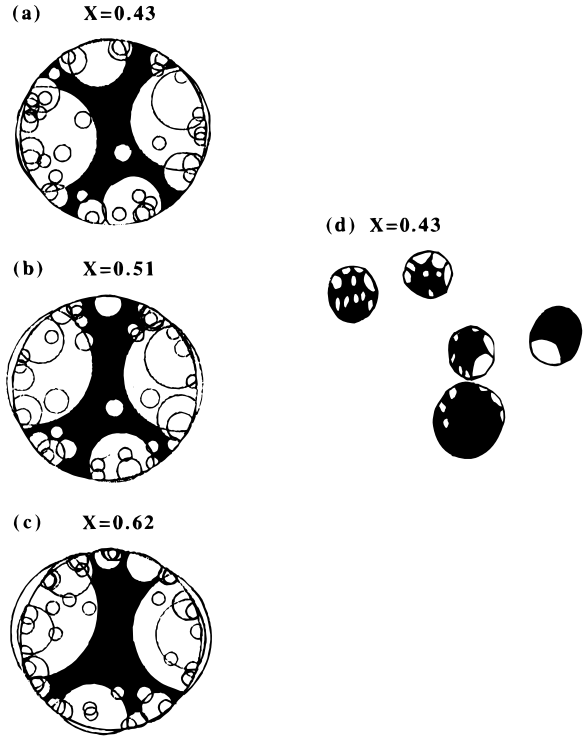

Figure 4. Comparison of the middle stages of the evolution of the particle morphology predicted by the model for run 1 in Table 1 (a−c) and the experimental morphology observed by Chen et al.[17] (d).

morphology observed by Chen et al.[17] It can be seen that, at low conversions, the model predicts that only a small number of clusters is formed in the polymer particle because, as shown in the phase diagram (line a in Figure 2), a large part of polymer 1 is dissolved in the polymer 2 matrix. Comparison with the experimental results reported by Chen et al.[17] suggests that the

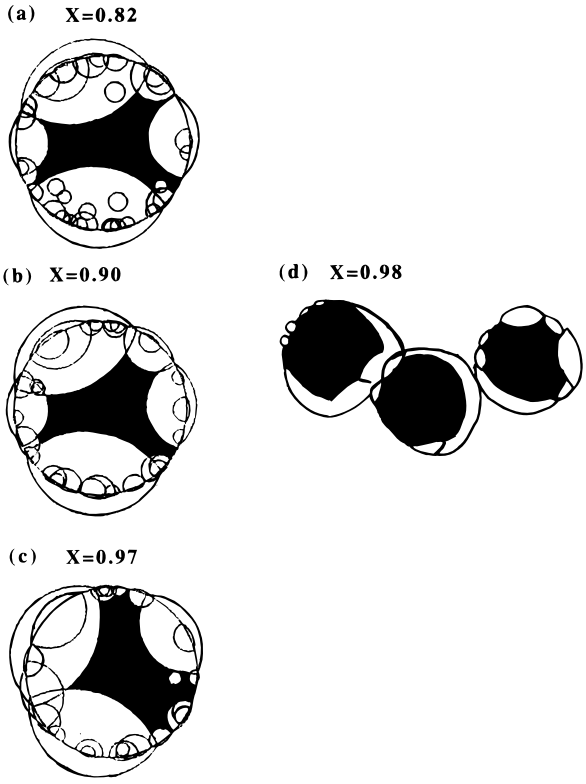

Figure 5. Comparison of the final stages of the evolution of the particle morphology predicted by the model for run 1 in Table 1 (a−c) and the experimental morphology observed by Chen et al.[17] (d).

actual MMA−pSt−pMMA system was less compatible than that represented by line a in Figure 2. However, it seems also possible that, because of the evaporation of monomer, some demixing might occur during the preparation and examination of the sample by TEM. If this is the case, then the experimental sample should be compared with the morphologies predicted by the model for higher conversions. A fairly good agreement between experimental observations and model predictions would be achieved under these conditions. During the initial stages, the clusters migrated toward the center of the polymer particle, i.e., the equilibrium morphology was an inverted core shell. Later the morphology evolved toward the occluded morphology. This behavior was due to the effect of monomer swelling on the interfacial tensions that in turn influenced the Hamaker constants.[1,26]

Figure 4 presents the evolution of the particle morphology predicted by the model for the middle stages of run 1 and a scheme of the particle morphology observed by Chen et al.[17] It can be seen that a fairly good agreement between the experimental results and model predictions was achieved. This figure shows that big clusters were formed by cluster coagulation and that new small clusters were nucleated.

Figure 5 presents the evolution of the particle morphology predicted by the model during the final stages of the polymerization together with the particle morphology observed by Chen et al.[17] for $X = 0.98$ using the embedded-in-ice technique. It can be seen that the model predicted a particle with big clusters of pMMA located near the surface in a close similarity with the experimental observation. It has to be pointed out that, in agreement with the experimental results, a metastable particle morphology was predicted by the model at the end of the polymerization. Therefore, the final particle morphology was determined by kinetic factors.

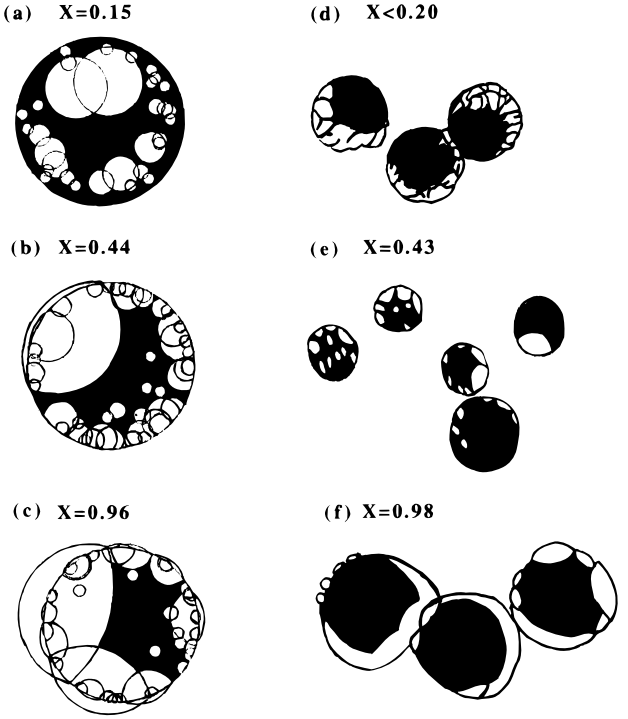

Figure 6. Comparison of the evolution of the particle morphology predicted by the model for run 1 in Table 1 using the phase diagram given by the line b in Figure 2 (a−c) and the experimental morphology observed by Chen et al.[17] (d−f).

In long enough times, the particle morphology reached the equilibrium morphology (occluded).

To investigate the effect of the polymer compatibility, run 1 was also simulated using the phase diagram given by line b in Figure 2. The results are presented in Figure 6, where a comparison with the morphologies observed by Chen et al.[17] was included. It can be seen that the initial morphology predicted by the model is much closer to the experimentally observed one than that obtained with the more compatible system (Figure 3). On the other hand, comparison between Figures 5 and 6 shows that polymer compatibility has only a limited influence on the final particle morphology.

Runs 2 and 3 in Table 1 tried to mimic the polymerization of MMA on a polystyrene seed reported by Jönsson et al.[21] These authors used different amounts of an oil-soluble initatior (lauroyl peroxide) to study the effect of the polymerization rate on particle morphology. TEM microphotographs of 60 nm thick ultratomed sections of the final latex particles were presented. In the calculations, the different initiator concentrations were accounted for by using different values of $\bar{n}$ that were chosen to have polymerization times similar to the experimental ones. It was assumed that the phase diagram in Figure 2, line a can be used for this process.

Figure 7 presents the evolution of the particle morphology predicted by the model for run 2 in Table 1 (reaction with the higher amount of initiator), as well as the drawing summarizing the main features of the morphology of the particles observed by Jönsson et al.[21] The simulated figures are projections of 60 nm thick sections (±30 nm around the maximum section of the particle) of the polymer particle. Figure 7 shows that the model predicts a slow cluster nucleation rate at the beginning of the process due to the considerable part of polymer 1 dissolved in the polymer matrix. Cluster nucleation and growth continued during the whole process. For this particular system, clusters migrate toward the surface of the particle. In the simulated

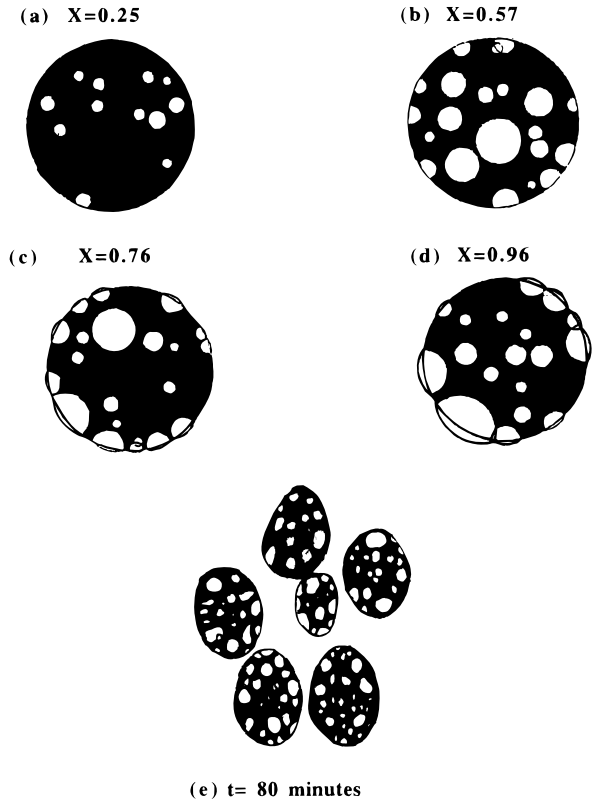

Figure 7. Evolution of the particle morphology predicted by the model for run 2 in Table 1 (a−d) and particle morphology experimentally observed by Jönsson et al.[21] (e).

figures, it seems that, in some cases, the total amount of material in the clusters decreased with conversion (for example, from $X = 0.57$ to $X = 0.76$). This simply means that some clusters, that at $X = 0.57$ were located in the 60 thick section represented in the figures, because of migration left this section by the time in which the conversion reached $X = 0.76$. Figure 7 shows that, at the end of the polymerization, many clusters remained inside the polymer particle, i.e., a metastable morphology was obtained. Figure 7 also shows that there is a good agreement between the final particle morphology predicted by the model and the one experimentally observed by Jönsson et al.[21]

Figure 8 presents the evolution of the particle morphology predicted by the model for run 3 in Table 1. This run corresponds to the polymerization carried out by Jönsson et al.[21] using a low amount of initiator. This was a slow reaction that was complete in about 10 h. In this simulation, $\bar{n}$ was adjusted to achieve high conversion in this time. The simulated figures are also projections of 60 nm thick sections of the polymer particle. It can be seen that clusters migrated toward the surface of the particle and that, due to the long process time, the final morphology was relatively close to the equilibrium occluded morphology. In addition, Figure 8 shows that a fairly good agreement between model predictions and experimental results was achieved. Comparison between Figures 7 and 8 shows that the slower the polymerization rate, i.e., the lower $\bar{n}$, the closer the final particle morphology to the equilibrium one, because the clusters had enough time for migration.

Sensitivity Analysis

The simulations reported above were carried out using arbitrary values for V_C and k_n. To investigate the

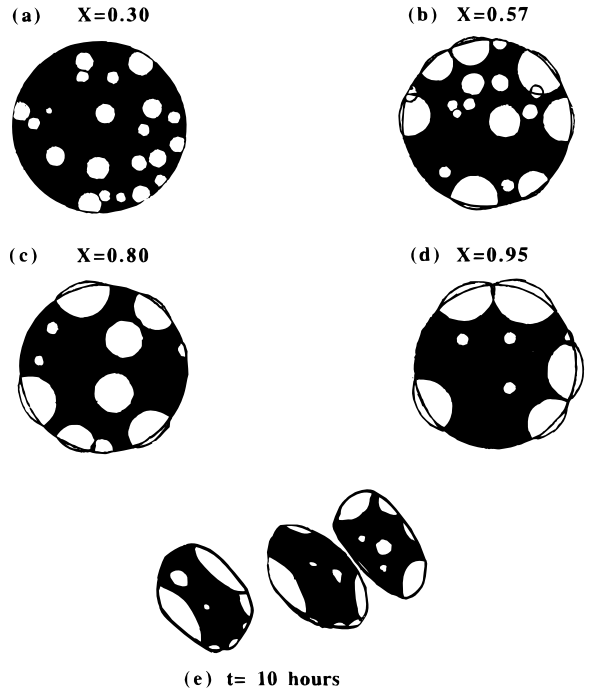

Figure 8. Evolution of the particle morphology predicted by the model for run 3 in Table 1 (a−d) and the particle morphology experimentally observed by Jönsson et al.[21] (e).

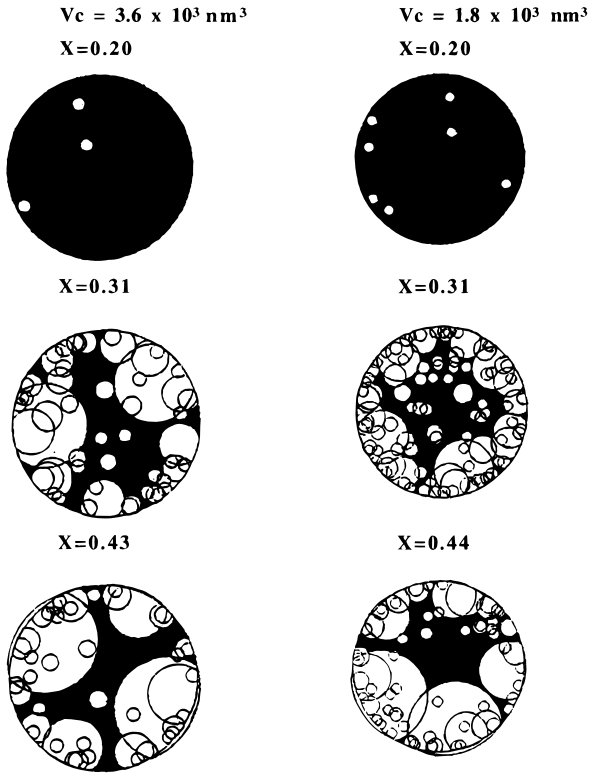

Figure 9. Effect of the initial cluster volume on the initial stages of the evolution of the particle morphology for run 1 in Table 1.

effect of the values of these parameters on the particle morphology some simulations were performed for the conditions of run 1 in Table 1. Figures 9 and 10 present the effect of the initial size of the cluster on the evolution of the particle morphology. It can be seen that the difference is significant during the initial stages of the process because more clusters are formed when the smaller initial cluster size is used. This difference is less pronounced during the middle stages and almost negligible at the end of the process (Figure 10).

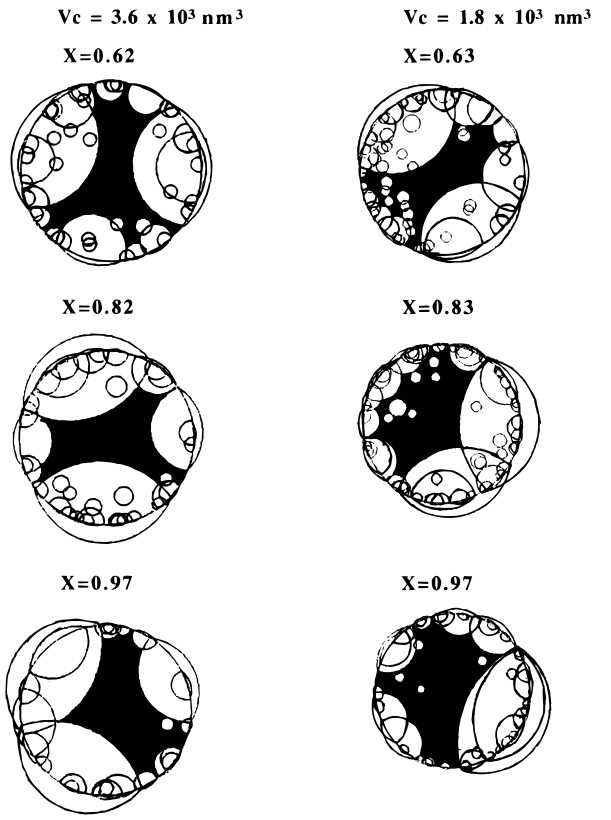

Figure 10. Effect of the initial cluster volume on the final stages of the evolution of the particle morphology for run 1 in Table 1.

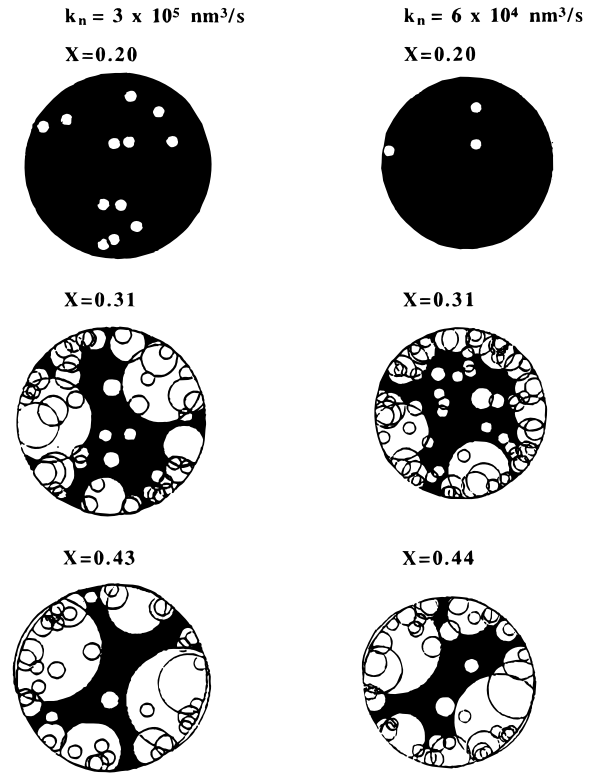

Figure 11. Effect of the cluster nucleation rate constant on the initial stages of the evolution of the particle morphology for run 1 in Table 1.

Figures 11 and 12 present the effect of the cluster nucleation rate constant on the evolution of the particle morphology. It can be seen that although some differences were observed at the beginning of the process, the final morphology was not affected by k_n.

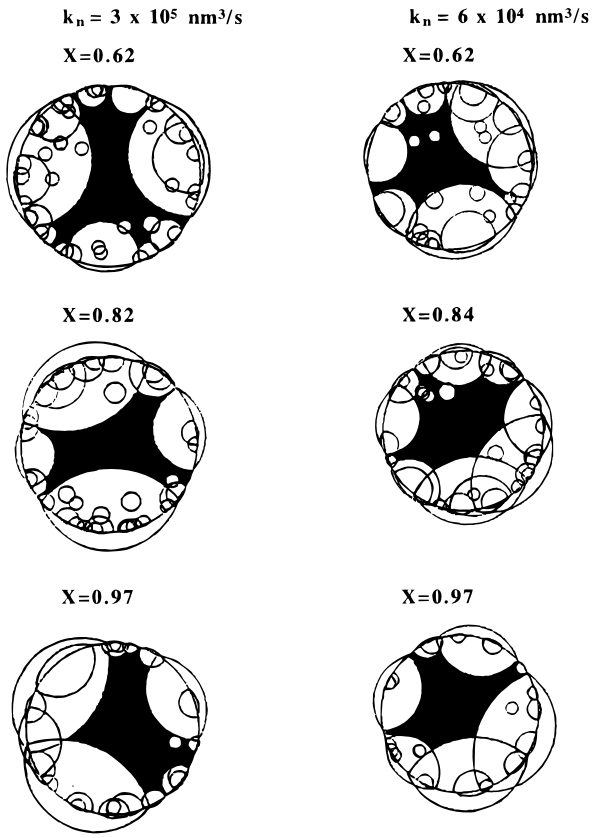

Figure 12. Effect of the cluster nucleation rate constant on the final stages of the evolution of the particle morphology for run 1 in Table 1.

Conclusions

A mathematical model for the development of the particle morphology in emulsion polymerization has been developed. The polymerization of monomer 1 on a seed of polymer 2 was considered. As polymerization proceeds, the concentration of polymer 1 in the particles increases and the phase separation, which leads to the formation of clusters, occurs. The model accounts for the kinetics of this process and places in a random way each new cluster in the polymer particle. Polymerization occurs in both the polymer matrix and the cluster. The concentrations of the monomer in the different phases are given by the thermodynamic equilibrium. The polymers are allowed to diffuse between phases. The clusters migrate toward the equilibrium morphology due to the balance between the van der Waals forces and the viscous forces. The model has been used to simulate some batch emulsion polymerizations of MMA on a polystyrene seed, for which the experimentally observed particle morphologies have been reported in the literature. It was found that the final particle morphology depends heavily on kinetic factors. Furthermore, the slower the polymerization rate, the closer the final morphology to the equilibrium one. A fairly good agreement between experimental results and model predictions was achieved. On the other hand, sensitivity analysis showed that the final particle morphology was not significantly affected by either the initial cluster volume or the cluster nucleation rate constant.

Acknowledgment. The AECI-UPV fellowship for L.J.G.-O. and the financial support by the Diputación Foral de Gipuzkoa are gratefully appreciated.

Nomenclature

A empirical constant required to calculate the critical concentration of demixing (−)

a_j matrix−cluster interfacial area (m^2)

B empirical constant required to calculate the critical concentration of demixing (−)

b_j friction factor (m)

C polymer concentration (kg/m^3)

C_R reference concentration of polymer 2 (kg/m^3)

d_{seed} diameter of the seed particle (m)

E_j energy of interaction of cluster j (J)

E_μ energy of activation for the viscosity of polymer solutions (J/mol)

$\mathbf{F}_j$ net van der Waals force acting on cluster j (N)

$\mathbf{F}_{jh}$ force acting on cluster j resulting from the interaction between clusters j and h (N)

$\mathbf{F}j3$ force acting on cluster j resulting from the interaction between cluster j and the aqueous phase (N)

F_{M_1} molar feed rate of monomer 1 (mol/s)

k Boltzmann's constant (J/mol K)

$k_{d_i}^1$, $k_{d_i}^2$ diffusion constants of the polymer i (m/s)

k_n nucleation constant (m^3/s)

k_p propagation rate constant (m^3/mol s)

M molecular weight of the polymer 2 (g/mol)

M_R reference molecular weight of the polymer 2 (g/mol)

M_1 amount of monomer 1 in the reactor (mol)

$[M_1]_i$ concentration of monomer 1 in phase i (mol/m^3)

$[M_1]_m$ concentration of monomer 1 in the polymer matrix (mol/m^3)

$\bar{n}$ average number of radicals per particle (−)

N theoretical number of clusters nucleated (−)

N^* actual number of cluster nucleated (−)

N_A Avogadro's number (molecules/mol)

N_P total number of polymer particles in the reactor (−)

P_M molecular weight of monomer (g/mol)

R_g radius of gyration (m)

t time (s)

T temperature (K)

T_R reference temperature (K)

V_C initial volume of the cluster (m^3)

v_j volume of cluster j (m^3)

v_m volume of the polymer matrix (m^3)

v_P volume of the monomer-swollen particle (m^3)

X conversion (−)

$\bar{X}_i$ ratio between the volume of a molecule of component i and a reference volume (−)

$\mathbf{X}_j$ vector giving the position of the cluster j at a given time (m)

$\mathbf{X}_{j0}$ vector giving the position of the cluster j starting a given integration step (m)

Greek Symbols

ϕ_i^j volume fraction of polymer i in point j(−)

χ_{0i} interaction parameter between the monomer and the polymer i (−)

χ_{12} interaction parameter between both polymers, per segment of polymer 1 (−)

χ_i adjustable parameter (−)

ρ_{p_1} density of polymer 1 (kg/m^3)

μ viscosity of the polymer matrix (Pa s)

μ_0^* reference viscosity (Pa s)

σ_{i3} interfacial tension between the monomer swollen phase i and the aqueous phase (N/m)

σ_{i3}^* interfacial tension between the polymer i and the aqueous phase (N/m)

σ_{M3}^* interfacial tension between the monomer and the aqueous phase (N/m)

σ_{12} interfacial tension between the monomer swollen polymeric phases (N/m)

References and Notes

(1) González-Ortiz, L. J.; Asua, J. M. *Macromolecules* **1995**, *28*, 3135.
(2) Grancio, M. R.; Williams, D. J. *J. Polym. Sci.: Part A-1* **1970**, *8*, 2617.
(3) Keusch, P.; Graff, R. A.; Williams, D. J. *Macromolecules* **1974**, *7*, 304.
(4) Chern, C.-S.; Poehlein, G. W. *J. Polym. Sci., Polym. Chem. Ed.* **1987**, *25*, 617.
(5) de la Cal, J. C.; Urzay, R.; Zamora, A.; Forcada, J.; Asua, J. M. *J. Polym. Sci., Polym. Chem. Ed.* **1990**, *28*, 1011.
(6) Mills, M. F.; Gilbert, R. G.; Napper, D. H. *Macromolecules* **1990**, *23*, 4247.
(7) Yang, S. I.; Klein, A.; Sperling, L. H.; Cassasa, E. F. *Macromolecules* **1990**, *23*, 4582.
(8) Croxon, C. A.; Mills, M. F.; Gilbert, R. G.; Napper, D. H. *Macromolecules* **1993**, *26*, 3563.
(9) Torza, S.; Mason, S. G. *J. Colloid Interface Sci.* **1970**, *33*, 67.
(10) Sundberg, D. C.; Casassa, A. P.; Pantazopoulos, J.; Muscato, M. R.; Kronberg, B.; Berg, J. *J. Appl. Polym. Sci.* **1990**, *41*, 1425.
(11) Chen, Y.-C.; Dimonie, V. L.; El-Aasser, M. S. *J. Appl. Polym. Sci.* **1991**, *42*, 1049.
(12) Chen, Y.-C.; Dimonie, V. L.; El-Aasser, M. S. *Macromolecules* **1991**, *24*, 3779.
(13) Winzor, C. L.; Sundberg, D. C. *Polymer* **1992**, *33*, 3797.
(14) Durant, Y. G. J.; Guillot, J. *Colloid Polym. Sci.* **1993**, *271*, 607.
(15) Sundberg, E. J.; Sundberg, D. C. *J. Appl. Polym. Sci.* **1993**, *47*, 1277.
(16) Daniels, E. S.; Dimonie, V. L.; El-Aasser, M. S.; Vanderhoff, J. W. *J. Appl. Polym. Sci* **1990**, *41*, 2463.
(17) Chen, Y.-C.; Dimonie, V. L.; El-Aasser, M. S. *J. Appl. Polym. Sci.* **1992**, *45*, 487.
(18) Chen, Y.-C.; Dimonie, V. L.; El-Aasser, M. S. *Pure Appl. Chem.* **1992**, *64*, 1691.
(19) Chen, Y.-C.; Dimonie, V. L., Shaffer; O. L.; El-Aasser, M. S. *Polym. Int.* **1993**, *30*, 185.
(20) Muscato, M. R.; Sundberg, D. C. *J. Polym. Sci., Polym. Phys. Ed.* **1991**, *29*, 1021.
(21) Jönsson, J.-E. L.; Hassander, H.; Jansson, L. H.; Törnell, B. *Macromolecules* **1991**, *24*, 126.
(22) Jönsson, J.-E. L.; Hassander, H.; Törnell, B. *Macromolecules* **1994**, *27*, 1932.
(23) Okubo, M.; Katsuta, Y.; Matsumoto, T. *J. Polym. Sci., Polym. Lett. Ed.* **1980**, *18*, 481.
(24) Min, T. I.; Klein, A.; El-Aasser, M. S.; Vanderhoff, J. W. *J. Polym. Sci., Polym. Chem. Ed.* **1983**, *21*, 2845.
(25) Hergeth, W.-D.; Bittrich, H-J.; Eichhorn, F.; Schlenker, S.; Schmutzler, K.; Steinan, U.-J. *Polymer* **1989**, *60*, 1913.
(26) González-Ortiz, L. J.; Asua, J. M. *Macromolecules* **1996**, *29*, 383.
(27) Perrin F. *J. Phys. Radium* **1934**, *VII* (10), 497.
(28) Resnick, R.; Halliday, D. *Física*; Continental: Ciudad de México, México, 1983; Chapter 8.
(29) Broseta, D.; Leibler, L.; Kaddour, L. O.; Strazielle, C. *J. Chem. Phys.* **1987**, *87*, 7250.
(30) Siow, K. S.; Patterson, D. *J. Phys. Chem.* **1973**, *77*, 356.
(31) Van Krevelen, D. W. *Properties of Polymers*; Elsevier: Amsterdam, 1990; Chapters 15 and 16.
(32) Hsu, C. C.; Prautsnitz, J. M. *Macromolecules* **1974**, *7*, 320.
(33) Flory, P. J. *Principle of Polymer Chemistry*; Cornell University Press: New York, 1953, Chapter XIII.
(34) Walling, C. *Free Radicals in Solution*; Wiley-Interscience Publication: New York, 1957.

MA960022Z